Low-Power Photothermal Self-Oscillation of Bimetallic Nanowires
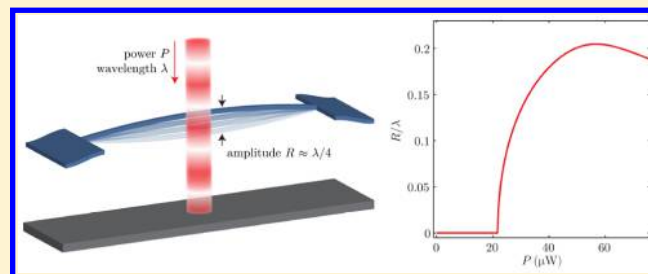
Roberto De Alba,[†][ID] T. S. Abhilash,[†] Richard H. Rand,[‡,§] Harold G. Craighead,[∥] and Jeevak M. Parpia[*,†]

[†]Department of Physics, [‡]Department of Mathematics, [§]Sibley School of Mechanical and Aerospace Engineering, and [∥]School of Applied and Engineering Physics, Cornell University, Ithaca, New York, 14853, United States

S Supporting Information

ABSTRACT: We investigate the nonlinear mechanics of a bimetallic, optically absorbing SiN−Nb nanowire in the presence of incident laser light and a reflecting Si mirror. Situated in a standing wave of optical intensity and subject to photothermal forces, the nanowire undergoes self-induced oscillations at low incident light thresholds of <1 μW due to engineered strong temperature-position $(T-z)$ coupling. Along with inducing self-oscillation, laser light causes large changes to the mechanical resonant frequency ω_0 and equilibrium position z_0 that cannot be neglected. We present experimental results and a theoretical model for the motion under laser illumination. In the model, we solve the governing nonlinear differential equations by perturbative means to show that self-oscillation amplitude is set by the competing effects of direct $T-z$ coupling and $2\omega_0$ parametric excitation due to $T-\omega_0$ coupling. We then study the linearized equations of motion to show that the optimal thermal time constant τ for photothermal feedback is $\tau \rightarrow \infty$ rather than the previously reported $\omega_0 \tau = 1$. Lastly, we demonstrate photothermal quality factor (Q) enhancement of driven motion as a means to counteract air damping. Understanding photothermal effects on nano- and micromechanical devices, as well as nonlinear aspects of optics-based motion detection, can enable new device applications as oscillators or other electronic elements with smaller device footprints and less stringent ambient vacuum requirements.

KEYWORDS: Nanomechanical systems, optomechanics, photothermal force, self-oscillation, nonlinear dynamics, parametric feedback

Micro- and nanomechanical resonators are widely studied for applications including electromechanical circuit elements and sensing of ultraweak forces,[1] masses,[2] and displacements.[3] An integral part of these systems is the detection method employed to readout motion, which must itself be extremely sensitive and inevitably imparts its own force on the resonator, influencing the dynamics. The phase relation between mechanical motion and the resulting detector back-action determines whether this interaction will serve to dampen vibrations or amplify them, potentially leading to self-oscillation if the detector supplies enough energy per cycle to overcome mechanical damping.

Feedback due to external amplifiers has been used to generate self-oscillation of micromechanical resonators;[4−8] in such systems the oscillation amplitude R is set either by nonlinearity of the amplifier or of the resonator. Similarly, systems in which mechanical motion influences the amount of laser light circulating in an optical cavity[9−12] or magnetic flux through a Superconducting QUantum Interference Device[13,14] (SQUID) have also been shown to self-oscillate under the right experimental conditions. In these systems, R is set largely by the periodicity of the detection scheme, either $R \approx \lambda/4$ where λ is the laser wavelength or $R \approx \Phi_0/2$ where Φ_0 is the displacement needed to change the SQUID flux by one flux quantum. In the case of a mechanical resonator coupled to an optical cavity, back-action can arise either from radiation pressure or photothermal force, that is, thermally induced deflection caused

by optical absorption. The effects of these two forces are identical if the cavity resonance (with frequency Ω_c and width κ) is sufficiently broad;[11,12,15−19] however if κ is much smaller than the mechanical vibration frequency ω_m the optomechanical system is said to be in the "sideband-resolved regime," and radiation-pressure effects are greatly enhanced at laser frequencies of $\Omega_c \pm \omega_m$.[20,21] Radiation-pressure-based feedback with red detuning $(\Omega_c - \omega_m)$ is currently one of the most promising experimental techniques for suppressing thermal motion and thereby accessing quantum behavior in mechanical systems.[22] Such low-κ optical systems can, however, be difficult to attain and miniaturize.

Photothermal feedback places less stringent requirements on the optical system (as we show in this work), and has been explored in a broad range of mechanical device geometries through experiment,[9,10,12,18,23−26] simulation,[27,28] and theoretical studies.[10,23,29] While these works provide many insights into the underlying physics, some neglect the thermally induced change in resonator equilibrium position z_0, while others neglect the change in resonant frequency ω_0. In this work, we have developed bimetallic nanowires that are designed to be especially susceptible to the photothermal force—devices in which optically induced changes to z_0 and ω_0 cannot be
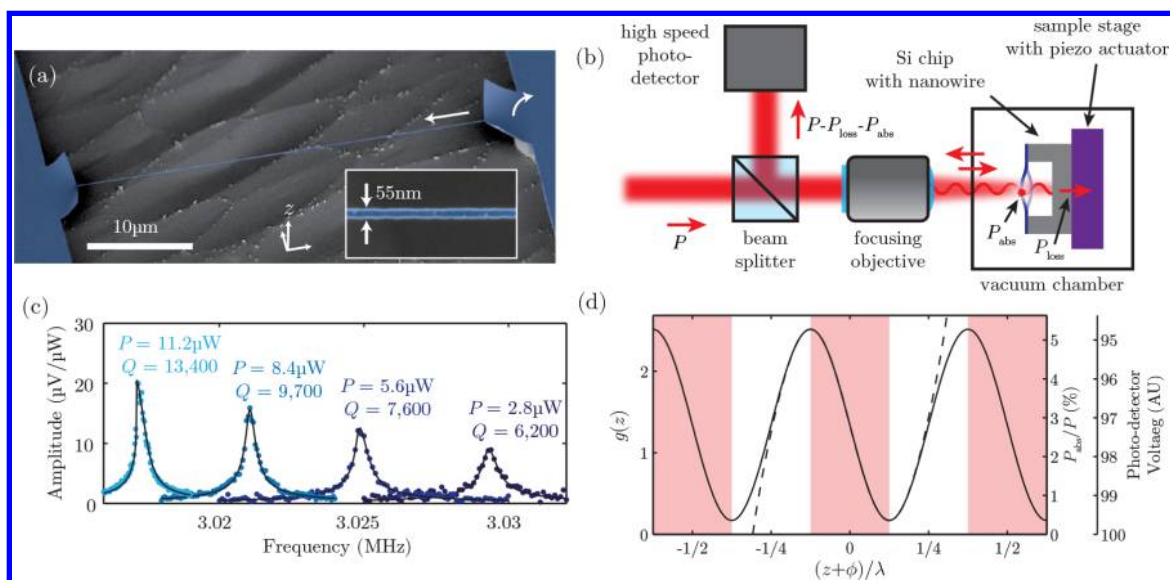
Figure 1. Optomechanical system and experimental setup. (a) False-color scanning electron micrograph of our suspended device; blue, the SiN/Nb bilayer. Arrows indicate the competing tensile force and bimetallic "torque" that provide dz/dT coupling. Inset: magnified top-down image of the nanowire. (b) The experimental setup: nanowire absorption modulates the reflected laser power, which is recorded by a high-speed photodetector. (c) Nanowire resonance at laser powers below the threshold for self-oscillation, driven inertially by a piezo actuator and sampled at 10 Hz; solid lines are Lorentzian fits. Considerable frequency softening $d\omega_0/dT$ and Q-enhancement can be seen as P increases. (d) The optical intensity profile $g(z)$ versus distance $z + \phi$ to the Si mirror. Because the nanowire is much narrower than the incident laser beam, only ~3% of laser light interacts with the nanowire; of this 3%, the nanowire absorbs ~70%. Self-oscillation occurs if the static nanowire is located in a shaded region and the power P is sufficiently high. A dashed line indicates the Taylor-series approximation for $g(z)$ used in the perturbation theory.
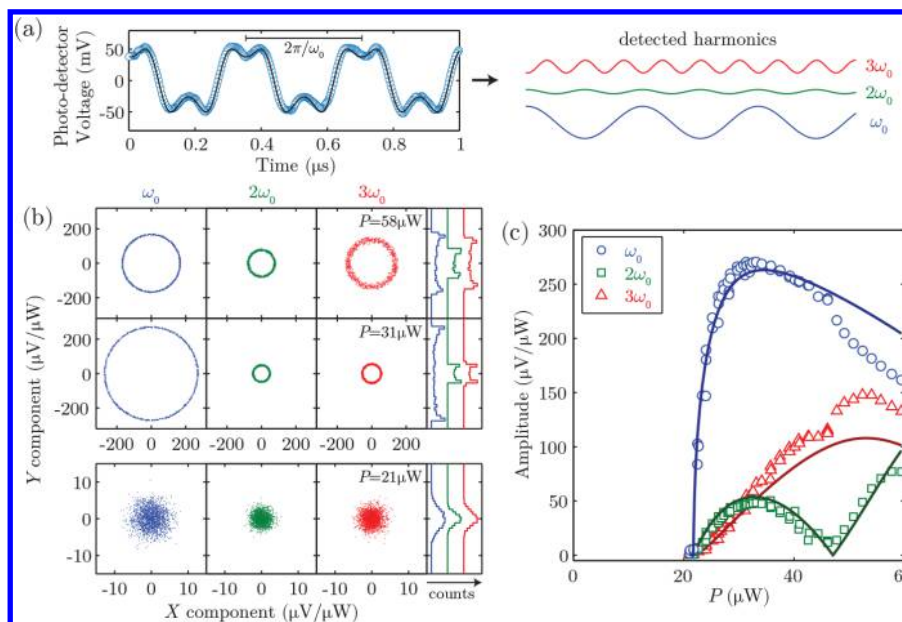

Figure 2. Photothermal self-oscillation. (a) Measured photodetector signal during nanowire self-oscillation (circles), and its decomposition into Fourier components (solid lines). Although the nanowire motion is a near-pure sinusoid, the nonlinear optical readout results in detected harmonics at integer multiples of the oscillation frequency. (b) Phase portraits of undriven nanowire motion as measured in the frequency domain by a multichannel lock-in amplifier centered about the resonant frequency. X and Y denote cosine and sine components of motion. The critical power needed for self-oscillation is $P_{crit} = 22$ μW. Data below this power (lowest row) is a combination of thermal motion and detector noise, while data above this power (upper rows) has a well-defined nonzero amplitude. Right-most panels are histograms along the Y axis. (c) Data points: amplitudes of the self-oscillation signals shown in (b) versus laser power P. Solid lines are a best fit based on the IPT model described in the text.

neglected. Temperature-position coupling dz/dT is provided by supporting bimetallic cantilevers at either end of the nanowire (shown in Figure 1a) and induces self-oscillation as well as changes in z_0. Differential thermal contraction within the cantilevers after metal deposition results in a permanent displacement of the nanowire above its original plane of fabrication; this displacement changes if the nanowire tension is altered (e.g., by heating). Temperature−frequency coupling $d\omega_0/dT$, also due to changing tension, produces an overall shift in ω_0 (Figure 1c) and modifies motion through $2\omega_0$ parametric excitation of the resonant frequency. We adapt the perturbation theory first discussed in ref 10 and present our results for a

general optical intensity profile $g(z)$. We then linearize the governing coupled z,T equations to study nanowire behavior at laser powers below the threshold for self-oscillation.

Our optomechanical system is depicted in Figure 1a,b. The nanowire consists of a 40 μm × 55 nm × 25 nm (length × width × thickness) layer of high-stress Si_3N_4 onto which 20 nm of Nb was deposited by sputtering. Low pressure chemical vapor deposition (LPCVD) Si_3N_4 was chosen for its high Q factors[30] and ease of processing, and Nb was chosen for future low-temperature experiments in which its superconductivity will be utilized; for the present experiment, any optically absorptive material will suffice. The extremely high aspect ratio (~1000:1, length/cross-section) of the nanowire enable it to easily achieve out-of-plane deflections on length scales comparable to our laser wavelength while also maintaining a low thermal mass, and thus achieving higher temperatures for a given laser power. By etching the underlying bulk Si to a depth of 8 μm in a timed KOH bath, the nanowire is suspended above a reflecting back-plane. Incident laser light ($1/e^2$ beam diameter $d_L \approx 2.5 \mu$m) is focused near the wire center and reflects off of the underlying Si to form a standing wave of optical intensity; our one-mirror optical system thus functions similarly to a very low-finesse two-mirror cavity. Focusing is performed using a 10× microscope objective with 34 mm working distance and NA = 0.28 (Mitutoyo M Plan objective). The total optical power (or more precisely, the electric field energy density $|\vec{E}(z)|^2$) in a plane parallel to the mirror at a distance z is given by $Pg(z)$, where $g(z)$ is the dimensionless intensity profile and P is the incident beam power; all P values given throughout this work signify this total beam power. Because the nanowire is extremely narrow, it covers only a small fraction $f \approx 3\%$ of the incident beam by area and can therefore be assumed not to influence $g(z)$. It does, however, absorb a small portion of the local power $P_{abs} = afPg(z)$ (where a is its absorption coefficient), and nanowire motion generates fluctuations in the reflected laser beam that can be measured using a high-speed photodetector. If we denote by P_{loss} the power lost due to absorption by the Si mirror, the signal measured by our photodetector is proportional to $P−P_{loss}−P_{abs}$, as shown in Figure 1d. This detection method has the benefit of utilizing the same light that induces self-oscillation and is highly nonlinear for oscillation amplitudes $R \gtrsim \lambda/8$, where $\lambda = 640$ nm is the laser wavelength used. If the optical field profile $g(z)$ is known, this detector nonlinearity can be used to deduce the absolute size of mechanical motion.

Self-oscillation of the nanowire is shown in Figure 2. Measured in the time domain (Figure 2a), purely sinusoidal motion with $R \approx \lambda/4$ results in a detected signal that saturates as z traverses the extremes of $g(z)$. This results in detected harmonics of the vibration frequency that can readily be measured in the frequency domain. Figure 2b shows the nanowire motion as measured by a multichannel lock-in amplifier whose reference frequency is centered at the resonant frequency $\omega_0 \approx 2\pi \times 3$ MHz with a 10 kHz bandwidth for three different laser powers; the three harmonics shown (ω_0, $2\omega_0$, $3\omega_0$) were measured simultaneously. The reference frequency was adjusted at each power to follow the resonance. Nanowire motion is plotted as X and Y quadratures, or in-phase and $\pi/2$ out-of-phase components relative to a fixed phase. The lower panel displays nanowire motion just below the critical power (P_{crit} = 22 μW), which is a combination of thermal motion and electrical noise about the origin; this has the expected Gaussian distribution. As P is increased above P_{crit}, all

three harmonics demonstrate sharply defined nonzero amplitudes. This optically induced motion has a phase that randomly cycles through all possible angles at a rate much faster than the data acquisition rate of ~50 ms per point. All plots show 1000 data points except for the lower panels that each contain 2000 points. Figure 2c shows the amplitude of these harmonics ($\sqrt{X^2 + Y^2}$) for many values of P. Solid lines are a best fit (with a total of four free parameters) based on the model described below. Deviation of the fit at high powers could be due to aberrations of the standing wave $g(z)$ caused by the nanowire, which has been studied previously by refs 25 and 31. For the sake of simplicity, our fitting model neglects any influence of the nanowire on $g(z)$. All measured signals are normalized by P, the incident laser power.

The governing differential equations for the position and temperature of our photothermal system[10] are

$$\ddot{z} + \gamma\dot{z} + \omega_{0i}^2(1 + CT)(z - DT) = 0 \tag{1}$$

$$\dot{T} + \frac{1}{\tau}T = PAg(z) \tag{2}$$

Here z is the deflection of the nanowire midpoint (with $z > 0$ corresponding to motion away from the mirror), and ω_{0i} and γ are its intrinsic resonant frequency and mechanical damping at $P = T = 0$. T denotes the nanowire temperature above ambient and C, D are the changes in (squared) resonant frequency and position per unit temperature, respectively; the resonant frequency of this system thus depends on temperature as $\omega_0^2 = \omega_{0i}^2(1 + CT)$. The second equation above is Newton's law of cooling, where τ denotes the thermal diffusion time constant, and the right-hand-side describes the heat input from the incident laser. The parameter $A = af/\mu$ contains the nanowire's optical absorption a, thermal mass μ, and fractional laser coverage f. Although the temperature will vary along the length of the nanowire, we assume T to represent the temperature at its center and calculate the thermal parameters A, C, and D accordingly; detailed calculations of the parameters in eqs 1 and 2 are presented in Section S6 of the Supporting Information (SI).

If the nanowire does not interact appreciably with the incident laser, we can approximate the local optical field as

$$g(z) = \alpha - \beta \sin\left(\frac{4\pi(z + \phi)}{\lambda}\right) \tag{3}$$

where $\alpha \geq \beta \geq 0$ so that $g(z) \geq 0$, and ϕ is the $P = 0$ nanowire position within the standing wave. Note that we have expressed $g(z)$ such that the self-oscillation region (with $dg/dz < 0$, shown in Figure 1d) is centered about $z + \phi = 0$. If the incident light is approximated as a plane wave, we have $\alpha = 1 + r$ and $\beta = 2\sqrt{r}$ where r is the reflection coefficient of the mirror. If instead an incident Gaussian laser beam is assumed, the parameters α, β, and ϕ become functions of z which depend on the mirror reflectivity, the focused laser waist diameter, and the waist-mirror distance, among other parameters (see Figure S5 of the SI.). Throughout this work, in order to minimize the complexity of our data modeling we use the former (plane wave) assumption with $r \approx 0.35$ corresponding to single-crystal Si. This assumption of constant α, β, and ϕ is valid for the small deflections $z < \lambda/2$ studied.

In other device geometries, large mechanical resonators can generate significant internal and external optical reflections, producing a Fabry−Perot interference effect which results in

$g(z)$ having sharper peaks and wider valleys or skewing its peaks left or right. For this reason, we present our theoretical results for a general intensity profile $g(z)$. In all cases, however, $g(z)$ is periodic in $\lambda/2$.

During self-oscillation, our resonator displacement is well modeled by $z(t) = z_0 + R\cos(\omega t)$ where R, ω are the oscillation amplitude and frequency, respectively, and z_0 is the temperature-dependent equilibrium position. This last value can be estimated by solving eqs 1 and 2 for the case of a static nanowire, which give the implicit equation $z_0 = \tau DPAg(z_0)$. Near $P = 0$ this formula has only one solution for z_0, but more solutions emerge as P increases. For high enough P values, solutions nearest $z = 0$ can cease to be valid; this suggests that the static wire exhibits discontinuous jumps in z_0 as P is increased quasi-statically. The static solution to eqs 1 and 2 is studied further in SI Section S2. While the static solution for z_0 (and the corresponding temperature $T_0 = z_0/D$) is a useful starting point for analyzing the self-oscillating nanowire, in what follows we will show that typical oscillation amplitudes R produce sizable changes to T_0 (and z_0).

Although eqs 1−3 are nonlinear and cannot be solved exactly, perturbative methods can be applied. Here we employ the Poincaré-Lindstedt method, which requires scaling γ, C, and D in eq 1 by a small dimensionless parameter $\varepsilon \ll 1$. Equations 1 and 2 can then be solved for $z(t)$, $T(t)$, and ω (the self-oscillation frequency) to any desired order in ε. The method also requires approximating $g(z)$ by the first few terms of its Taylor series. We thus expand $g(z)$ about $z + \phi = 0$ and keep enough terms such that the optical field is accurately modeled over an entire period $|z + \phi| < \lambda/4$

$$g(z) \approx k_0 + k_1(z + \phi) + k_3(z + \phi)^3 + k_5(z + \phi)^5 + k_7(z + \phi)^7 \tag{4}$$

where $k_0 = \alpha$, $k_1 = -4\pi\beta$, $k_3 = (32/3)\pi^3\beta$, $k_5 = -(128/15)\pi^5\beta$, and $k_7 = (1024/315)\pi^7\beta$. A comparison of this approximation with the exact $g(z)$ is shown in Figure 1d. The perturbation theory is presented in its entirety in SI Section S1, but the main results are given below.

Using eq 4 and solving eqs 1 and 2 to order ε^1 gives the following equation for R

$$0 = c_0 + c_1 R^2 + c_2 R^4 + c_3 R^6 \tag{5}$$

where

$$c_0 = \frac{\omega_1^2 D}{1 + \omega_1^2 \tau^2} g_{z_0}^{(1)} + \frac{\gamma}{\tau^2 PA}$$

$$c_1 = \frac{\omega_1^2 D}{1 + \omega_1^2 \tau^2} \frac{g_{z_0}^{(3)}}{2^2 1! 2!} - \frac{\omega_{0i}^2 C}{1 + 4\omega_1^2 \tau^2} \frac{g_{z_0}^{(2)}}{2^1 0! 2!}$$

$$c_2 = \frac{\omega_1^2 D}{1 + \omega_1^2 \tau^2} \frac{g_{z_0}^{(5)}}{2^4 2! 3!} - \frac{\omega_{0i}^2 C}{1 + 4\omega_1^2 \tau^2} \frac{g_{z_0}^{(4)}}{2^3 1! 3!}$$

$$c_3 = \frac{\omega_1^2 D}{1 + \omega_1^2 \tau^2} \frac{g_{z_0}^{(7)}}{2^6 3! 4!} - \frac{\omega_{0i}^2 C}{1 + 4\omega_1^2 \tau^2} \frac{g_{z_0}^{(6)}}{2^5 2! 4!}$$

Here we have introduced $\omega_1^2 = \omega_{0i}^2(1 + CT_0)$ as the new resonant frequency and $g_{z_0}^{(n)}$ as the nth derivative of $g(z)$ evaluated at $z = z_0$. This result is hereafter referred to as the first order perturbation theory (FOPT) solution. The number of terms in eq 5 increases if more terms are kept in the Taylor

expansion eq 4 (following the clear pattern in $c_0...c_3$), however the terms shown are sufficient to accurately model our experimental data. We note that this equation assumes the resonator is in the self-oscillation regime and thus is only valid for laser powers at or above the critical threshold P_{crit}. Furthermore, despite eq 5 being a cubic function of R^2 (and thus having three complex solutions) with the Taylor expansion chosen (eq 4) only one solution for R will be purely real; if more terms are included in the expansion such that multiple periods of $g(z)$ are retained, multiple real solutions can exist, each of which describes a possible state of the system.

As shown in the derivation provided in the SI, the nanowire oscillation $z(t) = z_0 + R\cos(\omega t)$ results in temperature fluctuations in the form of a Fourier series $T(t) = T_0 + \sum_{n=1}^{\infty} T_{n\omega} \cos(n\omega t + \theta_n)$. Of this series, the two components $T_{1\omega}$ and $T_{2\omega}$ prove to be the most consequential. $T_{1\omega}$ leads to the terms in D in eq 5, while $T_{2\omega}$ leads to the terms in C. The effect of C is thus equivalent to parametric 2ω modulation of the resonant frequency, while the effect of D is more direct. Equation 5 also suggests that as z_0 changes, C terms dominate near points of $g(z_0)$ with even symmetry (extrema) while D terms dominate near points of odd symmetry (inflection points). However, a careful examination of the Lyapunov stability of this system (given in SI Section S4) shows that the nanowire will not self-oscillate in the case $D = 0$, $C \neq 0$. We therefore conclude that D initiates self-oscillation, while C only modifies it. Unlike other mechanical systems in which 2ω parametric modulation can induce oscillation,[32,33] C here is incapable of doing so because of the dependence of $T_{2\omega}$ on R; see the SI for more details. The onset of self-oscillation occurs when $R = 0$ in eq 5; this leads to $c_0 = 0$ and gives a critical laser power of

$$P_{\text{crit}} = -\frac{\gamma(1 + \omega_1^2 \tau^2)}{\omega_1^2 \tau^2 DAg_{z_0}^{(1)}} \tag{6}$$

This expression reveals the source of low critical power in our nanowire: a combination of low thermal mass (and hence large A), long thermal time constant $\omega_1 \tau \approx 400$, and large coupling $D = 1.64$ nm/K afforded by our cantilevers. Further, because γ, D, and A are all positive, a negative optical gradient is needed for self-oscillation. While the sensitivity of P_{crit} on τ is rather weak for $\omega_1 \tau > 1$, it is noteworthy that short time constants $\tau \to 0$ inhibit self-oscillation. We revisit this later in the paper where we discuss operation of the wires in the presence of N_2 gas.

As mentioned above, FOPT predicts a change in the time-averaged temperature of the nanowire due to self-oscillation. This addition to T_0 is

$$\delta T_0 = -T_0 + \tau PA \sum_{n=0}^{3} \frac{R^{2n} g_{z_0}^{(2n)}}{2^{2n}(n!)^2} \tag{7}$$

The nanowire equilibrium position thus relocates to $z_0 = D(T_0 + \delta T_0)$ during self-oscillation. Although one could proceed to order ε^2 in perturbation theory to account for this equilibrium shift, the resulting algebraic expressions quickly become cumbersome. An approach that is easier to implement and was used to fit the data in Figure 2c is to recursively perform FOPT while updating T_0 and z_0 with successive δT_0 values. Starting with the static nanowire solution ($z_0 = \tau DPAg(z_0)$), R and δT_0 are iteratively calculated until R converges on a fixed value and δT_0 converges on zero. This scheme is hereafter referred to as iterated perturbation theory (IPT). We find in practice that IPT converges most reliably if δT_0 is multiplied by
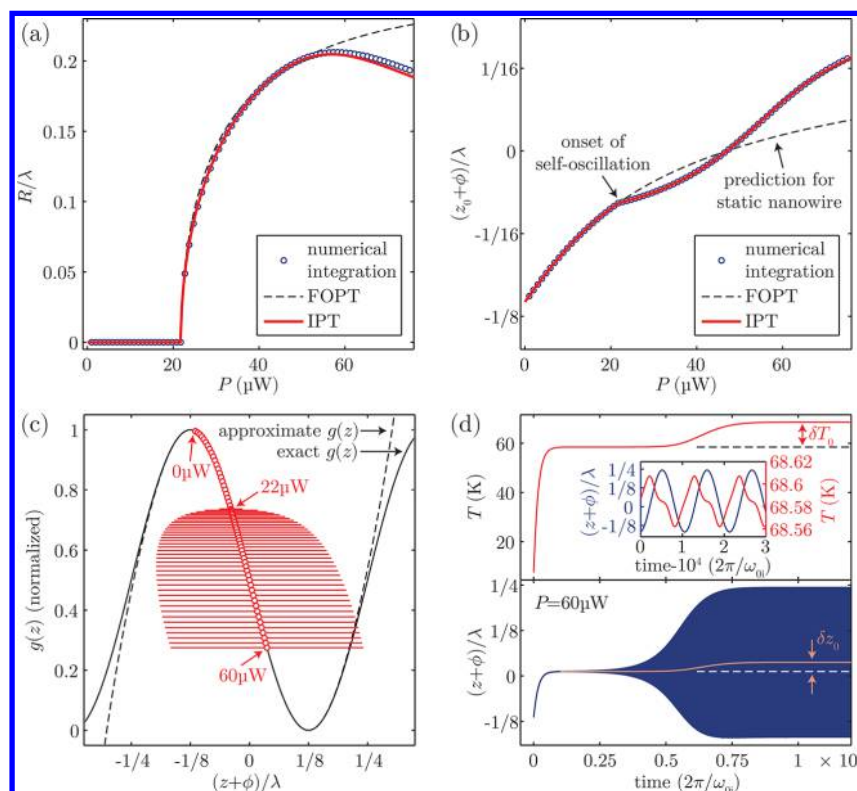
Figure 3. Detailed behavior of the nanowire according to fits of the experimental data. (a,b) Comparison of the oscillation amplitude R and equilibrium position z_0 calculated by perturbation theory and numerical integration with $\phi/\lambda = -0.114$. Note that $z_0 = 0$ at $P = 0$. The shift in z_0 due to self-oscillation is clearly visible in (b). (c) Nanowire position within the optical field $g(z)$ as P increases. Red circles (spaced every 1 μW) indicate the changing z_0 value, while horizontal lines indicate the extent of R. (d) Numerical integration results at $P = 60$ μW with the initial condition $(z, \dot{z}, T) = (0, 0, 0)$; only the upper and lower envelopes of oscillation are shown. In the lower panel, a solid line signifies the peak−peak moving average, which is an indication of z_0. The shift in z_0 after $t = 5 \times 10^3$ closely follows the trend in $T(t)$ shown in the upper panel. Inset: magnified image of these results near $t = 10^4$, showing the harmonic content of $z(t)$ and $T(t)$.

a small scaling factor (0.05 was used) before being added to T_0; convergence typically occurs within 20−100 iterations.

A comparison of FOPT, IPT, and numerical integration of eqs 1−3 is shown in Figure 3a,b. The parameters used are derived from the IPT fit to experimental data in Figure 2c; in this fit, the only free parameters were ϕ, τ, d_L, and an overall vertical scaling factor. It should be noted that while IPT reproduces the results of numerical integration almost exactly, IPT requires significantly less computation time and makes direct fitting of the experimental data possible; for numerical integration, each data point required a time-trace of several thousand cycles similar to that shown in Figure 3d. Figure 3c shows the nanowire position as it moves through the optical field. The deviation of z_0 away from its static value due to δT_0 is clearly visible in Figure 3b. Interestingly, z_0 trajectories from numerical integration and static theory intersect at $z_0 + \phi = 0$, that is, at the inflection point of $g(z)$; here the odd symmetry of $g(z)$ results in $\delta T_0 = 0$ in eq 7. The inflection point is crossed by z_0 at $P \approx 47$ μW, while the maximum R value occurs at the slightly higher power of $P \approx 56$ μW.

As shown in the numerical integration results of Figure 3d, self-oscillation requires roughly 10^4 oscillation cycles to reach steady state at $P = 60$ μW. Qualitatively, we observe that this "equilibration time" increases steadily for P values descending toward $P_{\text{crit}} = 22$ μW. Also shown in Figure 3d, the shift $\delta z_0 = 0.0251$ λ due to self-oscillation exactly matches the observed change in temperature $\delta T_0 = \delta z_0 / D = 10.1$ K, where $D = 1.64$ nm/K for this system. The magnified region in the Figure 3d

inset shows that during self-oscillation $z(t)$ is a nearly pure tone at frequency ω_1. Fourier analysis of this numerical data (not shown) reveals that the next largest harmonic component is $2\omega_1$, with 0.001% the amplitude of ω_1 motion. It is the pureness of this tone that leads to the excellent agreement between numerical integration and IPT; after all, the perturbation theory is predicated on the assumption $z(t) = z_0 + R \cos(\omega_1 t)$. Numerical results for $P > 60$ μW reveal that higher harmonics of the ω_1 motion grow steadily as P increases, possibly explaining the growing deviation from IPT seen in Figure 3a. While higher harmonics of motion do not significantly affect resonator dynamics for our present set of parameters, we note that their effect on the dynamics of an optical-cavity-coupled resonator are studied in detail in ref 34.

Perturbation theory can also be used to predict whether the onset of self-oscillation will be exhibit hysteresis. Such behavior is referred to as a subcritical Hopf bifurcation and would manifest as a continuation of stable self-oscillation for some range of powers as P is decreased below P_{crit}. The distinction between a hysteretic or nonhysteretic transition (subcritical or supercritical bifurcation) depends upon whether c_1 in eq 5 is negative or positive. Therefore

$$\frac{\omega_1^2 D g_{z_0}^{(3)}}{1 + \omega_1^2 \tau^2} < \frac{2\omega_{0i}^2 C g_{z_0}^{(2)}}{1 + 4\omega_1^2 \tau^2} \tag{8}$$

is the necessary condition for hysteresis. Because $C < 0$ in this experiment, we would expect hysteretic behavior when z_0 is
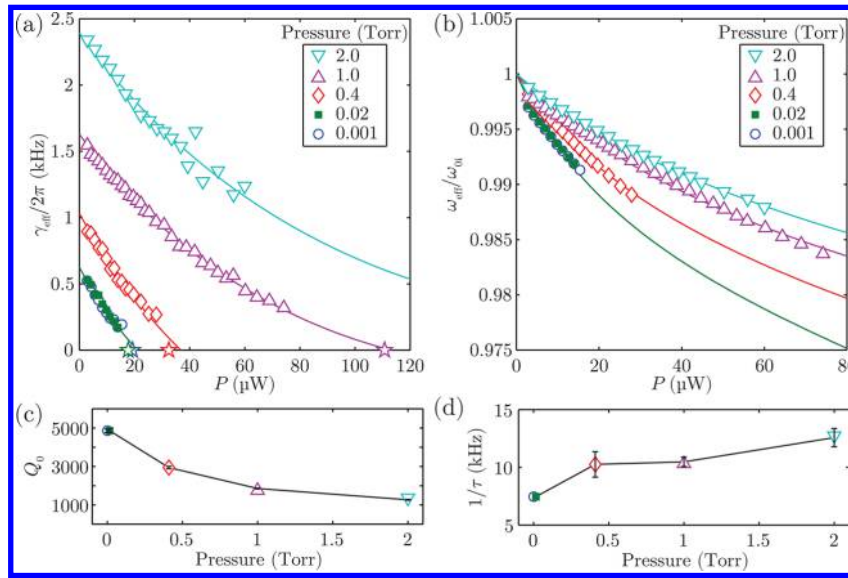
Figure 4. Nanowire behavior for $P < P_{crit}$ under various N$_2$ pressures. (a,b) Nanowire effective damping γ_{eff} and resonant frequency ω_{eff}. These values were obtained from Lorentzian fits to piezo-driven resonance peaks such as those shown in Figure 1c. Stars in (a) indicate the measured onset of self-oscillation. Solid lines are fits to eqs 11 and 12. (c) Q factors at $P = 0$ extrapolated from fits in (a,b). (d) Thermal diffusion rate $1/\tau$ versus gas pressure. Solid lines in (c,d) are guides to the eye, and errorbars denote $\pm 1\sigma$ (68%) uncertainty ranges from the fits.

near a maximum of $g(z)$. The width of the hysteresis region (i.e., how low P can be while still maintaining self-oscillation) is calculated in SI Section S3.

Lastly, we focus on the behavior of our nanowire for laser powers $P < P_{crit}$. Because the vibration amplitude in this case is typically much smaller than $\lambda/4$, it suffices to approximate $g(z)$ by a linear expansion about $z = z_0$ in eq 2: $g(z) \approx g(z_0) + g_{z_0}^{(1)}(z - z_0)$. Furthermore, because $T_{2\omega}$ is expected to be small, we can neglect any time-dependent CT terms in eq 1. This then leads to the linearized equations

$$\ddot{x} + \gamma \dot{x} + \omega_1^2(x - Du) = f_d e^{i\omega t} \tag{9}$$

$$\dot{u} + \frac{1}{\tau}u = PAg_{z_0}^{(1)}x \tag{10}$$

where we have introduced the new variables $x = z - z_0$, $u = T - T_0$ and added the driving term f_d at frequency ω. In this linearized system we can safely use the complex solutions $x = \tilde{x}e^{i\omega t}$ and $u = \tilde{u}e^{i\omega t}$. On the basis of eq 10, these are related by $u = x(\tau PAg_{z_0}^{(1)})/(1 + i\omega\tau)$. Substituting this into eq 9 and collecting real and imaginary terms, one can recast the mechanical system as $\ddot{x} + \gamma_{eff}\dot{x} + \omega_{eff}^2 x = f_d e^{i\omega t}$ where the effective resonant frequency ω_{eff} and damping γ_{eff} are

$$\omega_{eff}^2 = \omega_1^2\left(1 - \frac{\tau D P A g_{z_0}^{(1)}}{1 + \omega^2\tau^2}\right) \tag{11}$$

$$\gamma_{eff} = \gamma + \frac{\omega_1^2\tau^2 D P A g_{z_0}^{(1)}}{1 + \omega^2\tau^2} \tag{12}$$

First, we note that the photothermal terms in ω_{eff} constitute a roughly 1 part in 10^6 correction for the experimental parameters used in this work; thus to very good approximation $\omega_{eff} = \omega_1$. Next, we should expect self-oscillation to occur when $\gamma_{eff} = 0$. Substituting $P = P_{crit}$ from perturbation theory (eq 6) and $\omega = \omega_1$ indeed gives $\gamma_{eff} = 0$, showing compatibility of these two models. Interestingly, the photothermal damping shift on

resonance is $\Delta\gamma = |\gamma_{eff} - \gamma| \propto \frac{\omega^2\tau^2}{1 + \omega^2\tau^2}$, which increases monotonically as $\tau \to \infty$. Long time constants $\omega_1\tau \gg 1$ therefore strengthen the photothermal effect. This can also be seen by setting $\frac{1}{\tau} = 0$ in eq 10, which results in $u \propto ix$. In that case, u is perfectly out of phase with x, meaning it contributes entirely to damping in eq 9.

These results appear to be counter to those of previous theoretical studies which model the photothermal effect as a time-delayed back-action force $F(t) \propto \tau^{-1}\int_{-\infty}^{t} dt' I(x(t'))\exp[-(t - t')/\tau]$, where $I(x)$ is the position-dependent absorbed light intensity.[12,23] Such a model produces the result $\Delta\gamma \propto \frac{\omega\tau}{1 + \omega^2\tau^2}\frac{dF}{dx}$, which is maximized (in magnitude) when $\omega\tau = 1$ and vanishes as $\tau \to \infty$. The discrepancy here lies in dF/dx, which was previously treated as an unknown constant. Adapting our eqs 9 and 10 to such a model reveals that the thermal force magnitude (i.e., the asymptotic value of F after a change in x) is $F = kDu = kD\tau PAg_{z_0}^{(1)}x$, where k is the mechanical spring constant. This then leads to $\Delta\gamma \propto \frac{\omega^2\tau^2}{1 + \omega^2\tau^2}$, which is in agreement with our present result.

We have experimentally tested eqs 11 and 12 for several values of γ as shown in Figure 4. In these measurements γ was varied by introducing pure N$_2$ gas into our sample test chamber; doing so added drag to the nanowire motion, resulting in higher intrinsic damping γ and lowered Q factors (Figure 4c). All preceding measurements were performed with pressure $\ll 10^{-3}$ Torr. The fits shown in Figure 4a,b were constrained at the lowest two pressures to maintain consistent thermal parameters with the fit in Figure 2c. At higher pressures, τ was allowed to vary, as nanowire interaction with ambient gas likely increases its thermal dissipation rate. The laser spot diameter d_L and initial optical field position ϕ were also allowed to differ from Figure 2c as each change in pressure required manual refocusing, and the roughness of the Si backplane led to changes in ϕ based on laser positioning. Here $\phi/\lambda = 0.044$ compared to the value of -0.114 in Figure 2c; $d_L = 2.5$

μm for the two highest pressures and $d_L = 2.0$ μm for all lower pressures.

Curvature in the γ_{eff} and ω_{eff} fits is due to the changing equilibrium position z_0 as P increases, and the resulting change in $g_{z_0}^{(1)}$. Because of this curvature, the γ_{eff} trajectory for 2.0 Torr is not expected to enter self-oscillation at higher P values. It is however possible that if z_0 can extend to the next negative region of $g_{z_0}^{(1)}$, near $z + \phi = \lambda/2$, P would be large enough to support self-oscillation. We note that for the four values of pressure where self-oscillation is seen, the two lowest pressures yield P_{crit} and Q values consistent with no added N_2 gas. For the case of the two higher pressures, 0.4 and 1 Torr, the introduction of gas increases the damping (higher γ_{eff}) and shortens the τ, requiring an additional power to overcome damping. Above this pressure, self-oscillation cannot be reached in our present setup. Even so, the results of Figure 4 demonstrate the capability of photothermal feedback to counteract air damping at low pressures. Such optical Q-enhancement could lower the stringent vacuum requirements of typical microelectro-mechanical device applications.

We have presented an experimental and theoretical study of photothermal feedback in mechanical nanowires. While the device tested self-oscillates under the illumination of a 22 μW laser beam, only ~3% of this beam is incident on the ultrafine nanowire, suggesting that incident powers of <1 μW are ultimately necessary to induce motion. This is significantly lower than the 500 μW to few milliwatts required in previously studied free-space photothermal structures[10,35] and lower still than the ~10 μW reported for an optical-cavity-coupled photothermal structure,[12] where the two-mirror cavity produces much higher optical gradients dg/dz. The low power needed in our system is attributable to the low thermal mass of the nanowire and large temperature-position coupling D afforded by the supporting cantilevers. A simple beam-theory calculation suggests that D scales with cantilever length L and width W as L^3/W (see SI Section S7), suggesting that even stronger photothermal effects can readily be achieved. We have observed that the equilibrium position z_0 of this system is strongly tunable with incident laser power and can drastically affect nanowire dynamics. Self-oscillation in this system is due in part to temperature oscillations at the vibration frequency ω and to parametric 2ω oscillations of the resonant frequency. The perturbation theory used here can readily be adapted for systems in which micromechanical resonators are coupled to magnetic SQUID circuits, optical cavities, or other periodic external systems.

It is well established that a self-oscillating system can become entrained if a sufficiently strong driving force is applied, that is, the system will oscillate at the driver frequency rather than its own natural frequency.[9,36−39] Such a system is promising for a number of electromechanical applications, including narrow bandpass filters and related electrical signal processing devices. Although we have observed such behavior in our nanowires (not shown here), further work is needed to extend the perturbation theory to predict the entrainment bandwidth as a function of driver strength and laser power.

ASSOCIATED CONTENT

S **Supporting Information**

The Supporting Information is available free of charge on the ACS Publications website at DOI: 10.1021/acs.nano-lett.6b04769.

Full perturbation theory derivation of photothermal oscillation amplitude and frequency, including the potential for hysteresis. Theoretical analysis of the static nanowire behavior and Lyapunov stability of the static equilibrium. Details of device fabrication, and estimation of nanowire thermal parameters based on dimensions and materials used. Beam theory analysis of supporting cantilevers. Further information on the nonlinear optical readout scheme (PDF)

AUTHOR INFORMATION

Corresponding Author

*E-mail: jmp9@cornell.edu.

ORCID

Roberto De Alba: 0000-0003-1516-510X

Notes

The authors declare no competing financial interest.

REFERENCES

(1) Gavartin, E.; Verlot, P.; Kippenberg, T. J. *Nat. Nanotechnol.* **2012**, *7*, 509−514.

(2) Chaste, J.; Eichler, A.; Moser, J.; Ceballos, G.; Rurali, R.; Bachtold, A. *Nat. Nanotechnol.* **2012**, *7*, 301−304.

(3) Teufel, J. D.; Donner, T.; Li, D.; Harlow, J. W.; Allman, M. S.; Cicak, K.; Sirois, A. J.; Whittaker, J. D.; Lehnert, K. W.; Simmonds, R. W. *Nature* **2011**, *475*, 359−363.

(4) Feng, X. L. *Nat. Nanotechnol.* **2008**, *3*, 342−346.

(5) Weldon, J. A.; Alemán, B.; Sussman, A.; Gannett, W.; Zettl, A. K. *Nano Lett.* **2010**, *10*, 1728−33.

(6) Villanueva, L. G.; Karabalin, R. B.; Matheny, M. H.; Kenig, E.; Cross, M. C.; Roukes, M. L. *Nano Lett.* **2011**, *11*, 5054−5059.

(7) Chen, C.; Lee, S.; Deshpande, V. V.; Lee, G.-H.; Lekas, M.; Shepard, K.; Hone, J. *Nat. Nanotechnol.* **2013**, *8*, 923−927.

(8) Chen, C.; Zanette, D. H.; Guest, J. R.; Czaplewski, D. A.; López, D. *Phys. Rev. Lett.* **2016**, *117*, 017203.

(9) Zalalutdinov, M.; Zehnder, A.; Olkhovets, A.; Turner, S.; Sekaric, L.; Ilic, B.; Czaplewski, D.; Parpia, J. M.; Craighead, H. G. *Appl. Phys. Lett.* **2001**, *79*, 695−697.

(10) Aubin, K.; Zalalutdinov, M.; Alan, T.; Reichenbach, R. B.; Rand, R.; Zehnder, A.; Parpia, J.; Craighead, H. *J. Microelectromech. Syst.* **2004**, *13*, 1018−1026.

(11) Arcizet, O.; Cohadon, P. F.; Briant, T.; Pinard, M.; Heidmann, A. *Nature* **2006**, *444*, 71−74.

(12) Metzger, C.; Ludwig, M.; Neuenhahn, C.; Ortlieb, A.; Favero, I.; Karrai, K.; Marquardt, F. *Phys. Rev. Lett.* **2008**, *101*, 133903.

(13) Poot, M.; Etaki, S.; Mahboob, I.; Onomitsu, K.; Yamaguchi, H.; Blanter, Y. M.; van der Zant, H. S. J. *Phys. Rev. Lett.* **2010**, *105*, 207203.

(14) Etaki, S.; Konschelle, F.; Blanter, Y. M.; Yamaguchi, H.; van der Zant, H. S. J. *Nat. Commun.* **2013**, *4*, 1803.

(15) Kleckner, D.; Bouwmeester, D. *Nature* **2006**, *444*, 75−78.

(16) Gigan, S.; Bohm, H. R.; Paternostro, M.; Blaser, F.; Langer, G.; Hertzberg, J. B.; Schwab, K. C.; Bauerle, D.; Aspelmeyer, M.; Zeilinger, A. *Nature* **2006**, *444*, 67−70.

(17) Eichenfield, M.; Camacho, R.; Chan, J.; Vahala, K. J.; Painter, O. *Nature* **2009**, *459*, 550−555.

(18) Zaitsev, S.; Pandey, A. K.; Shtempluck, O.; Buks, E. *Phys. Rev. E* **2011**, *84*, 046605.

(19) Woolf, D.; Hui, P.-C.; Iwase, E.; Khan, M.; Rodriguez, A. W.; Deotare, P.; Bulu, I.; Johnson, S. G.; Capasso, F.; Loncar, M. *Opt. Express* **2013**, *21*, 7258−7275.

(20) Schliesser, A.; Arcizet, O.; Riviere, R.; Anetsberger, G.; Kippenberg, T. J. *Nat. Phys.* **2009**, *5*, 509−514.

(21) Aspelmeyer, M.; Kippenberg, T. J.; Marquardt, F. *Rev. Mod. Phys.* **2014**, *86*, 1391−1452.

(22) Chan, J.; Alegre, T. P. M.; Safavi-Naeini, A. H.; Hill, J. T.; Krause, A.; Groblacher, S.; Aspelmeyer, M.; Painter, O. *Nature* **2011**, *478*, 89−92.

(23) Metzger, C.; Favero, I.; Ortlieb, A.; Karrai, K. *Phys. Rev. B: Condens. Matter Mater. Phys.* **2008**, *78*, 035309.

(24) Ramos, D.; Mertens, J.; Calleja, M.; Tamayo, J. *Appl. Phys. Lett.* **2008**, *92*, 173108.

(25) Ramos, D.; Gil-Santos, E.; Pini, V.; Llorens, J. M.; Fernández-Regúlez, M.; San Paulo, Á.; Calleja, M.; Tamayo, J. *Nano Lett.* **2012**, *12*, 932−937.

(26) Barton, R. A.; Storch, I. R.; Adiga, V. P.; Sakakibara, R.; Cipriany, B. R.; Ilic, B.; Wang, S. P.; Ong, P.; McEuen, P. L.; Parpia, J. M.; Craighead, H. G. *Nano Lett.* **2012**, *12*, 4681−4686.

(27) Blocher, D.; Zehnder, A. T.; Rand, R. H.; Mukerji, S. *Finite Elements in Analysis and Design* **2012**, *49*, 52−57.

(28) Blocher, D.; Rand, R. H.; Zehnder, A. T. *International Journal of Non-Linear Mechanics* **2013**, *52*, 119−126.

(29) Restrepo, J.; Gabelli, J.; Ciuti, C.; Favero, I. *C. R. Phys.* **2011**, *12*, 860−870.

(30) Southworth, D.; Barton, R.; Verbridge, S.; Ilic, B.; Fefferman, A.; Craighead, H.; Parpia, J. *Phys. Rev. Lett.* **2009**, *102*, 225503.

(31) Ramos, D.; Gil-Santos, E.; Malvar, O.; Llorens, J. M.; Pini, V.; San Paulo, A.; Calleja, M.; Tamayo, J. *Sci. Rep.* **2013**, *3*, 3445.

(32) Mahboob, I.; Yamaguchi, H. *Nat. Nanotechnol.* **2008**, *3*, 275−279.

(33) Unterreithmeier, Q. P.; Weig, E. M.; Kotthaus, J. P. *Nature* **2009**, *458*, 1001−1004.

(34) Poot, M.; Fong, K.; Bagheri, M.; Pernice, W.; Tang, H. *Phys. Rev. A: At., Mol., Opt. Phys.* **2012**, *86*, 053826.

(35) Zalalutdinov, M.; Aubin, K. L.; Pandey, M.; Zehnder, A. T.; Rand, R. H.; Craighead, H. G.; Parpia, J. M.; Houston, B. H. *Appl. Phys. Lett.* **2003**, *83*, 3281−3283.

(36) Pandey, M.; Aubin, K.; Zalalutdinov, M.; Reichenbach, R. B.; Zehnder, A. T.; Rand, R. H.; Craighead, H. G. *J. Microelectromech. Syst.* **2006**, *15*, 1546−1554.

(37) Pandey, M.; Rand, R.; Zehnder, A. *Communications in Nonlinear Science and Numerical Simulation* **2007**, *12*, 1291−1301.

(38) Blocher, D. B.; Zehnder, A. T.; Rand, R. H. *J. Microelectromech. Syst.* **2013**, *22*, 835−845.

(39) Wang, H.; Dhayalan, Y.; Buks, E. *Phys. Rev. E: Stat. Phys., Plasmas, Fluids, Relat. Interdiscip. Top.* **2016**, *93*, 023007.